Mica-liquid trace elements partitioning and the granite-pegmatite connection: The St-Sylvestre complex (Western French Massif Central)

Arnaud Villaros, Michel Pichavant

Journal Pre-proof

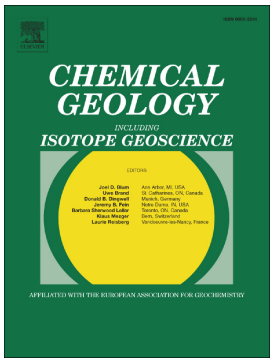

Mica-liquid trace elements partitioning and the granite-pegmatite connection: The St-Sylvestre complex (Western French Massif Central)

A. Villaro, M. Pichavant

PII: S0009-2541(19)30367-5

DOI: https://doi.org/10.1016/j.chemgeo.2019.07.040

Reference: CHEMGE 19265

To appear in: *Chemical Geology*

Received date: 15 January 2019

Revised date: 16 April 2019

Accepted date: 31 July 2019

Please cite this article as: A. Villaro and M. Pichavant, Mica-liquid trace elements partitioning and the granite-pegmatite connection: The St-Sylvestre complex (Western French Massif Central), *Chemical Geology* (2019), https://doi.org/10.1016/j.chemgeo.2019.07.040

Mica-liquid trace elements partitioning and the granite-pegmatite connection: The St-Sylvestre complex (Western French Massif Central)

Villaros A.[1*], Pichavant M.[1]

Univ. d'Orléans, ISTO, UMR 7327, 45071, Orléans, France ; CNRS, ISTO, UMR 7327, 45071 Orléans, France ; BRGM, ISTO, UMR 7327, BP 36009, 45060 Orléans, France

*arnaudvillaros@gmail.com

Submission to Chemical Geology

Keywords: granite-pegmatite connection, granitic melt composition, LCT pegmatite, mica crystallization, trace elements

Abstract

We constrain the genetic relation between granite and pegmatite parental melts from the Variscan Saint Sylvestre leucogranite complex and associated pegmatite bodies (Massif Central, France) through compositions of micas. Using mica trace element concentrations and available partition coefficients for Li, Rb, Ba, Cs and F, we calculated the trace element contents of granitic and pegmatitic melts at equilibrium with micas. Biotite in leucogranites and pegmatites ranges mostly from Fe-biotite to siderophyllite. More evolved facies contain protolithionite and zinnwaldite and lepidolite occurs in the most fractionated pegmatite. White micas have homogeneous compositions, from muscovite to Li-phengite. In granites, biotite and muscovite trace element distributions are clustered. In pegmatites, mica trace element contents globally follow differentiation from the least to the most evolved body. The reconstructed pegmatitic and granitic melts present strong compositional similarities such as enrichments in Li, Rb, Cs and depletion in Ba that suggest a similar origin. However, micas are shown to have selectively equilibrated with the last melt (or fluid) in contact and so trace element concentrations of early magmatic liquids are rarely preserved. Inversion of the mica data constrains the composition of parental melts and the trace element evolutions during crystallization. Leucogranite and pegmatite melts show mutual incompatible element evolutions inconsistent with a parent-daughter genetic relation. The data and the modelling suggest that they represent non-cogenetic melts generated by discrete episodes of partial melting. Differentiation is thus inherited from source processes rather than being the consequence of fractional crystallization of a common parental melt/magma. We suggest that both the leucogranites and the pegmatites originate from partial melting of a heterogeneous source rather than pegmatites being the product of granite crystallization.

1 Introduction

Differentiation through fractional crystallization is commonly proposed to explain the peculiar enrichments of rare metals and volatiles in granitic and pegmatitic magmas. For instance, differentiation of two-micas granite is believed to generate fractionated rocks which include rare-element enriched leucogranites (e.g. Raimbault et al. 1995, Charoy and Noronha, 1996, Breiter et al. 1997, Linnen, 1998) and pegmatites (Linnen et al 2012, London, 2012, Hulsbosch et al. 2014). For pegmatites, such a genetic model has several requirements: 1) A simple geometric relationship: the most differentiated magmas should be found farther from the parental granite, producing a distinctive spatial and compositional zonation (e.g., Černý and Ercit, 2005; London, 2005; Linnen et al., 2012). 2) The proximity between the parental granites and the residual magmas. 3) A relative chronology supporting a continuous crystallization process with the most differentiated magma being of the same age or younger than the parental granite. 4) A limited timeframe allowing the persistence of residual melt. 5) Geochemical evidence for progressive enrichment of incompatible elements, rare metals and volatiles from the granite to the most evolved pegmatite magma. Yet, numerous pegmatite fields do not comply with these requirements, either because of chronological discrepancy (e.g. Deveaud et al 2013 and 2015; Goodenough et al. 2014; Melleton et al. 2015) or of geometries that conflict with the fractionation model (e.g. London, 2005, Simmons, 2008). This stresses the need for either upgrade of the fractional crystallization model or the building of an alternative model. In that matter, an origin of pegmatite through direct small degree of partial melting has been often suggested (Nabelek et al. 1992a; b; Roda-Robles et al. 1999; Romer et al., 2014; Simmons et al. 1995, 1996, 2008; Shaw et al., 2016). According to this model, the high degrees of enrichment in incompatible elements and rare metals in pegmatite would result from partial melting of crustal sources.

In order to distinguish between the two models above on a geochemical basis, the most common approach has been to use whole rock compositional data combined with spatial and temporal relationships (e.g., Barros et al., 2016; Shand et al 2016). However, studying granite differentiation or examining the granite-pegmatite connection on the basis of whole-rock data can be problematic. Indeed, granites are end products of crystallization and they hardly directly reflect the evolution of melt composition (e.g., McCarthy and Groves, 1979). As a consequence, the liquid line of descent, and

thus the evolution from the primary (least fractionated) to the residual (most fractionated) melt is unknown. In the same way, due to pegmatite zonation and crystal sizes, representative sampling and whole rock analysis of pegmatite is not straightforward and, so, comparing granite and pegmatite whole-rock compositions can be fraught with difficulties. Finally, hydrothermal reworking below the solidus can lead to whole-rock compositions unrepresentative of their magmatic evolution (e.g., Pollard et al. 1987, Kontak, 2006, Muller et al., 2006). Alternatives to the use of whole-rock compositions include melt inclusion and obsidian studies (Pichavant et al., 1987a; Webster et al., 1997; Thomas and Davidson, 2012), but these can be applied only to a few systems, thus limiting their practical use. A more general approach, yet rarely applied to granitic systems, consists in using minerals to access the liquid composition (Hanson, 1978, Bea et al., 1994, London, 2015). Assuming that no post-magmatic re-equilibration occurred, provided that mineral/melt partition coefficients are available and appropriate for the system being considered, the composition of the melt at equilibrium with a mineral (n.b., melt and liquid are used interchangeably below) can be theoretically determined if the composition of the mineral is known. The obtained compositional trends can thus be used to constrain genetic relations between the different melts. In particular, incompatible trace elements allow to distinguish between (1) cogenetic liquids related through fractional crystallization, which show a single linear trend from parental (C_0) to residual (C_f) compositions and (2) non-cogenetic liquids evolving by fractional crystallization independently from each other, which show parallel trends from C_0 to C_f (figure 1; Treuil and Joron, 1975; Raimbault et al., 1987; Shaw, 2006).

In this paper, we apply this approach by using the trace element compositions of micas to follow the geochemical evolution from two-micas leucogranite to pegmatite melts. The Variscan Saint Sylvestre leucogranite and pegmatite complex in the NW part of the French Massif Central (FMC) is selected as a test site. Results show that leucogranite and pegmatite melts are compositionally close and have undergone a similar evolution. However, the incompatible trace element contents of the respective liquids, reconstructed from compositions of micas, do not follow a single fractionation trend. Therefore, pegmatites cannot be considered as representing fractionation products from granitic

magmas, thus stressing the interest of the partial melting model as an alternative way to generate pegmatitic liquids.

2 Background, strategy and methods

2.1 Trace element contents of micas as indicators of the evolution of granitic and pegmatitic melts

Micas are classical indicators of the geodynamic environment of silicic igneous suites (Nachit et al., 1985; Abdel-Rahman, 1994). Mica major element compositions are probes of magma intensive parameters such as temperature and fO_2 (Wones and Eugster, 1965; Czamanske and Wones, 1973; Bucholz et al., 2018). In granitic rocks, micas crystallize in a wide range of environments and are, among major mineral phases, the main witnesses of the early crystallization history (Tischendorf et al., 1997). Recently, the development of high resolution analytical techniques has extended the use of mica compositions to trace elements (e.g., Kaeter et al., 2018; Legros et al., 2018; Zhu et al., 2018). Micas incorporate many rare elements such as Li, Be, B, Rb, Cs, Ba, Sn, Nb and Ta (Van Lichtervelde et al., 2008) which are potential indicators of the geochemical evolution. Here, we explore the use of mica trace elements to record the composition of their parental melts. Results are applied to resolve the genetic connection between granitic and pegmatitic melts.

Peraluminous felsic igneous rocks such as leucogranites and pegmatites both contain biotite and muscovite. According to experimental studies on leucogranitic compositions (e.g. Scaillet et al. 1995), biotite is the liquidus phase. Muscovite, on the contrary, is a later phase, crystallising near the solidus. As a consequence, biotite and muscovite can coexist during the course of crystallization of peraluminous leucogranitic and pegmatitic magmas and, so, they potentially record the evolution of melt trace element concentrations. Leucogranites and pegmatites include biotite-bearing muscovite-free and two-mica varieties as common lithological types. Biotite-free facies such as muscovite leucogranites and lepidolite pegmatites also occur (Scaillet et al., 1990; Nabelek et al., 1992). The NW

part of the FMC hosts large massifs where leucogranites and pegmatites are found in close spatial association. One is the Saint Sylvestre Leucogranite Complex (SSLC) which hosts the Mont d'Ambazac Pegmatite Field (MAPF), constituted of numerous pegmatitic bodies and which includes the rare metal- and lepidolite-bearing Chèdeville LCT pegmatite (Raimbault, 1998; Deveaud et al., 2015). This massif satisfies to the main criteria (geometry, distance, relative chronologies, see above and Deveaud et al., 2015) for suggesting a genetic connection between leucogranites and pegmatites. Consequently, it was selected as a test site for geochemical modelling.

In the following, mica compositions from leucogranites of the SSLC and associated pegmatites of the MAPF will be used to determine the composition of their equilibrium melts. In granitic rocks *sl*, micas offer better perspectives than feldspars (easily re-equilibrated at low temperatures, Pollard et al. 1987; Stemprok, 1987) and quartz (generally very pure except for only a few trace elements, Breiter et al., 2013) to achieve this goal. Focusing on a single phase (i.e., mica) rather than on multiphase assemblages (i.e., whole rock) greatly limits the complexity of the modelling. Compared to this latter approach, the former appears as a first necessary step. It is also more robust given the uncertainties in the mineral/melt *Kd* database (see below). Last, it has the advantage to eliminate issues about the significance of whole rock assemblages (e.g., McCarthy and Groves, 1979). Implicit in the approach is the assumption that micas preserve magmatic compositions. For muscovite, this assumption can be tested relatively easily from major elements (Miller et al., 1981). For biotite, distinguishing between magmatic and hydrothermal compositions requires a case-by-case evaluation. In the SSLC, previous studies including Li isotope data have indicated that biotite (and also muscovite) compositions globally reflect the magmatic evolution (Deveaud et al. 2015). However, Li-rich micas such as zinnwaldite and lepidolite (which are rare but present in some of our pegmatites) most probably have a dual (both magmatic and hydrothermal) origin (e.g., Raimbault, 1998) and these compositions will be distinguished from the others below.

2.2 Evaluation of the Kd database and limitations

During crystallization, trace elements partition between liquid and minerals. The incompatibility (or compatibility) of a trace element is expressed by the partition coefficient between a given mineral and the melt (*Kd* = concentration of trace element *i* in mineral / concentration of trace element *i* in melt). In principle, *Kd* varies with temperature, the nature and composition of the mineral, the liquid composition and certain compositional and intensive parameters such as fO_2 (e.g. Icenhower and London, 1995; Nash and Crecraft, 1985; McIntire, 1963; Pichavant et al, 2016).

Trace and minor elements considered in this study include Li, Rb, Nb, Ta, Ba, Cs and F, this choice being largely dictated by the availability of suitable partition coefficients. Focus is placed on the incompatible elements, Ba serving to illustrate the behaviour of compatible elements. Experimental mica/liquid partition coefficients used in this study are summarized in table 1, together with partition coefficients for other major phases. The mica/liquid *Kd* values were selected to come only from (1) experiments, (2) at temperatures between 750 and 620 °C and (3) at fO_2 between NNO-2 and NNO+3 (Icenhower and London, 1995; Pichavant et al., 1996). In the following, we use the entire range of *Kd* (minimum and maximum values selected using the three criteria above, table 1; figure 2) instead of a single value to derive compositions of equilibrium liquids. This has the disadvantage of increasing the dispersion of the calculated liquid concentrations. Despite being less sensitive, this approach is considered as more robust than the choice of a single value because it better accounts for the uncertainties in the available *Kd* database.

While the temperature range above is adequate for leucogranite, crystallization of pegmatitic melts commonly extends to lower than 620 °C (e.g., Pichavant et al., 1987b; Sirbescu and Nabelek, 2003; London, 2015). Owing to their different crystallization temperatures, partition coefficients may thus differ between pegmatite and leucogranite melts. Indeed, values in the *Kd* database vary with temperature **(table 1; figure 2**). For example, the *Kd* biotite/liquid for F and Li both decrease when lowering temperature from 720-750°C to 620°C. The *Kd* muscovite/liquid for Li drops by a factor > 5 between 650 and 620°C, but the lowest values correspond to charges more oxidized than the highest (Pichavant et al., 2016; Icenhower and London, 1995). For Rb, Ba and Cs, the data at 650°C show significant dispersions (figure 2). Given the variability in the *Kd* database, it is difficult to extract the

effect of temperature as would be necessary if leucogranite and pegmatite crystallization are to be modelled at different temperatures. Therefore, below, the same *Kd* range will be assumed to be equally applicable to leucogranite and pegmatite liquids.

Another factor to be considered for pegmatites is that they commonly crystallise under disequilibrium, i.e., from undercooled melts (e.g., London, 2015). This necessarily impacts the use of equilibrium partition coefficients, as done in this study. However, Morgan and London (2003) found no influence of the degree of undercooling on the partitioning of incompatible elements (Cs) between alkali feldspar and melt. For a strongly compatible element (Ba), the alkali feldspar/melt *Kd* was found to increase relative to the reference equilibrium value, although by < 1 order of magnitude (Morgan and London, 2003). Therefore, disequilibrium crystallization effects are expected for compatible (Ba) but not for incompatible elements which are the focus of this study. Overall, disequilibrium crystallization effects should be of minor importance in this study. We stress that this conclusion applies only to crystallization and not necessarily to other processes such as diffusive exchange (between minerals or minerals and fluid) that can affect trace element concentrations in micas and are fully considered below.

Several elements were tested as a differentiation index, especially Nb. However, the mica/liquid partition coefficient for Nb (and also for Ta), determined at temperatures outside the range defined above (Stepanov and Hermann, 2013), yields highly enriched, irrealistic liquid Nb (and Ta) concentrations. Consequently, below, the liquid concentration results for these two elements will not be discussed and only mica Nb and Ta concentrations will be used. Finally, Cs will be used below as a differentiation index.

3 Geological context

The SSLC is part of the Variscan orogen which is the consequence of a nappe stacking event between 360 to 320 Ma. This resulted in the superposition of 4 units, from top to bottom, the Thiviers-Payzac Unit (TPU), the Upper Gneiss Unit (UGU), the Lower Gneiss Unit (LGU) and finally the

Autochthonous Unit (PAU) (e.g. Faure et al, 2009). This nappe stacking episode was followed by a collisional stage and the collapse of the belt from 330 Ma to about 300 Ma, during which numerous peraluminous granitic bodies intruded the upper nappes. The Saint Sylvestre Leucogranite Complex (figure 3) was emplaced during the mid-carboniferous (324 ± 4 Ma, Holliger et al. 1986) at the end of the collisional stage of the Variscan orogen (Faure and Pons 1991; Le Carlier Le Veslud, 2013). The SSLC is a thin laccolith (2–3 km in thickness, Audrain et al. 1989) intrusive in the PAU and the LGU (Audrain et al. 1989; figure 3).

The SSLC is strictly composed of peraluminous leucogranites exclusively derived from the melting of continental crustal components (e.g. Vidal et al. 1984, Turpin et al 1990). It is divided in three units from west to east: the Brâme, the St Sylvestre and the St Goussaud Unit. The Brâme unit is mostly composed of the Brâme granite (γ_{Br}), a coarse to medium grained porphyritic biotite ± cordierite ± garnet granite. γ_{Br} is characterised by a flat lying foliation and the presence of migmatitic septa and xenolithic gneisses (Mollier and Bouchez, 1982; Mollier, 1984; Cuney et al., 1990). U-Pb data on monazite and zircon provide crystallization ages for γ_{Br} of 324 ± 4 Ma (Holliger et al 1986). The undeformed fine grained two-mica Châteauponsac granite (γ_{Ch}) intrudes γ_{Br} as N020 striking dykes and sills. The central St Sylvestre unit comprises three petrographical facies: a biotite ± muscovite facies (γ_1) a fine grained muscovite + biotite facies (γ_2) and an albite, muscovite ± sillimanite facies (Sagne, γ_{sa}). From γ_1 to γ_{sa}, the amounts of biotite and accessory phases decrease while muscovite and albite both increase; whole-rock contents of rare metals (Sn, W, Li, F, Be, U) increase and the Th/U ratio decreases. The contact between γ_1 and γ_2 suggest that both facies are nearly synchronous (Cuney et al., 1990; Scaillet et al 2006). In the following, γ_1 and γ_2 will be grouped together as the St Sylvestre granite (γ_{Sy}). Finally, the St Goussaud Unit is mostly composed of an apparently isotropic, large grained, two micas albitic leucogranite (γ_{Go}). γ_{Go} only contains very rare angular enclaves (Aréne and Autran, 1979).

Within the SSLC, a rare-element pegmatite field (the Mont d'Ambazac pegmatitic field, MAPF) mostly intrudes the coarse-grained γ_1 granite. Over one hundred pegmatitic bodies have been identified (Raimbault, 1998). According to the classification of Černý and Ercit (2005), pegmatites from the

MAPF belong to the beryl type of the Li - Cs - Ta (LCT) group. Ar-Ar ages of lepidolite from a highly differentiated pegmatite have yielded an age of 309 ± 0.9 Ma ($^{40}Ar/^{39}Ar$, Cheilletz et al. 1992). Although the available geochronological data indicate that the pegmatites are younger than the leucogranites, we stress the difference between dating methods (U/Pb and Ar-Ar respectively) and the composite nature of the SSLC. Deveaud et al. (2013 and 2015) has proposed a classification of MAPF pegmatites based on the observations of Patureau (1987) and the zoning criteria of London (2014). Six types, with mineral characteristics summarised in **table 2**, have been recognized.

Representative samples of the SSLC were collected and their whole-rock composition determined. Micas from the different granites were analysed in thin sections. Micas from pegmatite were collected from different samples representative of each type. Sampling was directed at intermediate units to make comparison possible between the different pegmatite types and also because most intermediate units contain a two-mica phase assemblage in addition to quartz and K-feldspar (Deveaud et al., 2015). Due to heterogeneous mica repartition and minimum crystal size requirements analysis, biotites and muscovites were commonly sampled up to metres away from each other and the analyses performed on mineral separates.

4 Analytical techniques

Whole rocks were analysed at SARM (CRPG, Vandœuvre-les-Nancy). Major element chemical compositions of micas were obtained using a SX-50 CAMECA electron microprobe (ISTO, Orléans). Analyses were performed at 15 kV, with a mean electron beam of 10 nA, a spot diameter between 3 and 5 μm, a counting time of 20 s on peak and of 20 s on backgrounds (lower and upper). Standards for calibration were albite (Si, Na, K), MgO (Mg), Al_2O_3 (Al), topaz (F), apatite (P), andradite (Ca), orthoclase (K), Fe_2O_3 (Fe), vanadinite (Cl), $MnTiO_2$ (Mn, Ti).

Trace elements were determined using a Agilent 7500 series laser ablation inductively coupled plasma mass spectrometry (LA-ICP-MS) at LMV (Clermont- Ferrand) using a Resonetics M-50E 193 nm ArF Excimer laser with a standard 30 cm² cell and 100 % He flushing (mixed with Ar + N_2 after the cell).

The laser beam was focused to yield either a 44 or a 58 µm spot, with energy of 5 J/cm² and 3 Hz repetition rate. Data were calibrated against the NIST 612 (Pearce et al 1997) glass which was analysed every 20 spots. A BCR® glass was used as a secondary standard. Accuracy is commonly better than 3 % except ^{7}Li and ^{181}Ta for NIST 612 (3.19% and 5.91 respectively). Precisions are strictly below 2 %. Details for sampling and analytical accuracy and precisions are provided in Electronic supplementary material 1.

5 Results

5.1 Whole-rock compositions

Granitic rocks (table 3) range from moderately ferromagnesian and aluminous (γ_{Br}) toward more aluminous and felsic compositions (γ_{Sa}, γ_{Go} and γ_{Ch}). The γ_{Sy} granite compositions are intermediate between γ_{Br} and γ_{Go} **(**figure 4). The intrusive granites (γ_{Ch} and γ_{Sa}) are the most differentiated with γ_{Sa} being the more felsic and γ_{Ch} the more aluminous (figure 4, electronic supplementary material 1). Trace element contents of selected samples (figure 4) show a continuous enrichment in Li, Cs, Rb and F, in agreement with the observed differentiation from γ_{Br} to γ_{Sa}. Thus, the whole-rock data suggest that these elements behave incompatibly. On the contrary, Ba concentrations decrease with Cs. The whole-rock Nb/Ta ratio diminishes with granite differentiation, with values from 10-20 in γ_{Br} down to 1 in γ_{Sa}, most samples ranging between 10 and 4. For comparison with granites, whole-rock compositions of aplitic and lepidolite units of one representative MAPF type VI pegmatite are given in table 3.

5.2 Major element composition of micas

Textural relationships in granite and pegmatite of the SSLC and MAPF suggest that micas, dioctahedral and trioctahedral, are both magmatic (Scaillet et al 2006; Deveaud et al., 2015). Therefore, in γ_{Sy}, γ_{Go}, γ_{Ch} as well as in most pegmatite types, two mica phases coexisted during crystallization. In leucogranites, apart from γ_{Br} which lacks muscovite and γ_{Sa} which lacks biotite, biotite and muscovite occur together either as isolated individual phases or as inclusions in quartz and feldspars. Biotite inclusions in muscovite can be also found. In pegmatites, muscovite is present in all types and the amount of biotite significantly decreases with differentiation from type II to VI. In type II, III and IV, biotite and muscovite form intergrowths and muscovite displays two main different textures (Deveaud et al., 2015). Zinnwaldite compositions appear from types IV and are present in type V and VI, the latter containing also lepidolite (Raimbault, 1998; Deveaud et al., 2015).

Mica structural formulae were calculated on a 22 O basis with Li_2O contents determined from LA-ICP-MS analysis. No chemical zonation was found within the analysed micas. Therefore, the compositional ranges observed for a given sample and mica (see below) reflect inter-crystal variability in the same thin section and not intra-grain zonation. Our major element data for muscovite and biotite in SSLC leucogranites (table 4) are similar to the results of Monier and Robert (1986) and Monier (1987). In general, biotite composition in leucogranites ranges from Fe-biotite to siderophyllite, overlapping with biotite in pegmatites (figure 5). Fe-biotites occur in less differentiated leucogranites (γ_{Sy} and γ_{Br}) and in type II pegmatite, while the most differentiated facies γ_{Ch} and γ_{Go} and type III pegmatite host Fe-biotite to siderophyllite. Trioctahedral micas in type IV and V pegmatites extend to more evolved compositions (protolithionite and zinnwaldite, figure 5) and lepidolite compositions are found in type VI. In comparison, compositions of white micas are more homogeneous, covering a small range from muscovite to Li-phengite. Again, the data for leucogranites and pegmatite overlap but the most evolved white micas are found in granite (γ_{Sa}, figure 5). Compared to granites, muscovites from pegmatites (irrespective of the two textures noted above) are intermediate between compositions in $\gamma_{Sy,}$ γ_{Go} and γ_{Ch} on the one hand and in γ_{Sa} on the other hand. The evolution towards increasing F and Li concentration in micas is progressively marked from γ_{Br} to γ_{Sa} and from the less toward the more

evolved pegmatite type. Deveaud et al. (2015) pointed out that such an evolution takes place under constant $^{7}Li/^{6}Li$ in muscovite and biotite.

5.3 Trace element composition of micas

Trace elements in micas are highly variable in both granite and pegmatite (table 4). In *granites*, concentrations are clustered: biotite from γ_{Br} and γ_{Sy} and both biotite and muscovite from γ_{Ch} and γ_{Go} form well-defined clusters (figure 6). Alike for whole rocks, incompatible element (Li, Cs or Rb) concentrations progressively increase with differentiation (i.e., with lowering Mg-Li in mica) while compatible element (e.g. Ba) and Nb/Ta concentrations decrease. The highest Li, Cs and Nb/Ta and the lowest Ba concentrations are recorded by white micas in γ_{Sa} (figure 6; Table 4). In γ_{Go}, Li contents are homogeneous in both biotite and muscovite, but Cs, Ba, Ta and Nb/Ta vary considerably. γ_{Ch} records different behaviours: the white mica data are tightly grouped but the biotite data show substantial variability in Ba and Nb/Ta. Finally, muscovites in γ_{Sa} are the phases that record a significant and systematic enrichment in all incompatible elements (figure 6) and also in Ta (table 4), correlated with a Ba depletion (figure 6). The evolution of trace element concentrations from biotite to muscovite within a given sample is variable. For F, Li, Cs, Rb and Ba, concentrations in biotite are mostly equal (γ_{Sy}), and sometimes higher (γ_{Ch}) than in coexisting muscovite.

In *pegmatites*, the trace elements contents (table 4) globally agree with the evolution proposed by Deveaud et al. (2013, 2015). Contents in incompatible elements (Li, Cs and Ta) progressively increase with differentiation (i.e., from type II to VI), while contents in compatible elements (Ba) decrease. More in detail, biotite in type II pegmatite contains homogeneous Li and more variable Cs, Ba and Ta. Type III and IV pegmatites have micas with rather homogeneous trace element contents. Li, Cs, Rb and Ta are higher or equal (Ba) in biotite than in muscovite. Micas from Type V show the same type of behaviour for Li, Cs, Rb and Ta; however, for Ba, some concentrations are higher in muscovite than in biotite. It is worth stressing that the database for type V pegmatites includes one point for biotite and three different (and grouped) points for zinnwaldite (figure 6). Muscovite is also quite variable in

Li, Ba and Ta. Finally, lepidolite from type VI pegmatite records the most extreme concentrations with Ba contents < 5 ppm, Ta from < 50 to > 200 ppm and Cs in the 1000-200 ppm range (figure 6).

Mica Nb/Ta ratios behave in two different ways, being either homogeneous (γ_{Br}, γ_{Sy}, $\gamma_{Ch,}$ type II) or highly variable (γ_{Go}, γ_{Sa}, type III, IV, VI) in both muscovite and biotite. The range of Nb/Ta values is similar in micas in granites and pegmatites. Homogeneous values are between 10 and 20, whereas variable values range either from > 2 to ~40 in granites and from < 1 to < 20 in pegmatites (figure 6). Samples containing lepidolite and zinnwaldite have low Nb/Ta values (< 5). Interestingly, biotite and muscovite can record similar Nb/Ta as for example in γ_{Sy} and γ_{Ch}. In γ_{Go}, higher Nb/Ta are found in biotite than in muscovite whereas the opposite appears in pegmatites, i.e., muscovite in type V records higher Nb/Ta values than biotite and zinnwaldite.

6 Discussion

6.1 Micas as recorders of differentiation processes

6.1.1 Leucogranites

Trace element compositions of granitic liquids calculated using mica/liquid partition coefficients are plotted as a function of the Nb/Ta ratio of micas (figure 7). In figure 8, their variations with $[Cs]_{liq}$ used as a differentiation index are detailed. The data are also detailed for each granite separately (electronic supplementary material 2). Several differentiation mechanisms can be identified.

(1) White micas in γ_{Go} and γ_{Sa} are characterized by low (< 10) and highly variable Nb/Ta ratios correlated with either constant ($[Li]_{liq}$) or increasing ($[Rb]_{liq}$, $[Cs]_{liq}$, $[Ba]_{liq}$) concentrations (figure 7). When plotted as a function of $[Cs]_{liq}$, incompatible elements ($[Rb]_{liq}$) increase while $[Li]_{liq}$ stays almost constant and $[F]_{liq}$ (n.b., F is compatible in micas, table 1) show little variations (figure 8). $[Ba]_{liq}$ show an unexpected behaviour (e.g., slight positive correlation with $[Cs]_{liq}$, figure 8). We note that the variations in Nb/Ta (and the associated trace element evolutions) are marked mostly on white micas

(i.e., on late-crystallising phases) and are specific of the two most fractionated leucogranites. Since these variations are also encountered in most pegmatites (figure 6), differentiation processes responsible for these Nb/Ta variations are discussed in the pegmatite section (6.1.2). What is important for the present purpose is that these trace element patterns result from mechanisms late in granite crystallization histories.

(2) The γ_{Go} and γ_{Sa} data indicate a more "equilibrated" behaviour for $[Li]_{liq}$ than for $[Rb]_{liq}$, $[Cs]_{liq}$ and $[Ba]_{liq}$ (figure 7). At the crystal scale, trace element concentrations are homogeneous. However, in γ_{Sa}, at the thin section scale, the different muscovite crystals analysed record homogeneous $[Li]_{liq}$ (and, in γ_{Go}, the different biotite and muscovite crystals record identical $[Li]_{liq}$) whereas Nb/Ta, $[Rb]_{liq}$, $[Cs]_{liq}$ and $[Ba]_{liq}$ all vary to different extents depending on sample and mica (figure 7). Thus, Li shows a specific behaviour, attributed to its particularly high mobility. In silicate liquids at 1000 K, the diffusivity of Li is ~$10^{2.8}$ times higher than Rb and ~$10^{5.6}$ times higher than Cs (Zhang et al 2010). Diffusion data for micas are scarce (Sr: 10^{-21} m².s-1 at 700°C, Hammouda and Cherniak, 2000; Rb: 10^{-19} m².s-1 at 650 °C, Hoffman and Giletti, 1970) but, in albite at 1000 K, the diffusivity of Li is ~10^{9} times higher than Rb (Cherniak, 2010). This suggests the possibility to homogenise Li in micas by diffusive equilibration with either a Li-rich residual liquid or an intergranular fluid, alternatively. Large cations such as Rb, Cs and Ba generally have lower diffusivities. This limits equilibration between crystals for these elements and, so, micas in the same thin section can record a range of melt (or fluid) compositions, as illustrated by the γ_{Go} and γ_{Sa} data (figure 7). This indicates that a mechanism of selective equilibration of micas with the last melt (or fluid) in contact is operative.

(3) For biotites and muscovites in γ_{Br}, γ_{Sy} and γ_{Ch}, and biotites in γ_{Go}, grouped and "normal" unfractionated Nb/Ta are found (figure 7). Li being excepted for reasons explained above, no systematic evolution appears between trace element liquid compositions calculated from biotite (C_L^{bi}) and from muscovite (C_L^{mu}). For γ_{Sy}, apart from an outlier which is the consequence of an anomalously low biotite Cs concentration (see figure 6), $C_L^{bi}$are respectively higher (Cs, Rb) and lower (Ba) than the C_L^{mu} (figure 7; figure 8). For γ_{Ch}, C_L^{bi} and C_L^{mu} are both in the same range (figure 8; electronic supplementary material 2). Thus, muscovite in two-mica leucogranites records either less evolved (γ_{Sy})

or similar (γ_{Ch}) trace element concentrations than biotite. γ_{Go} is the only granite with indications for liquid compositions at equilibrium with biotite being less evolved than at equilibrium with muscovite (C_L^{bi} respectively equal or lower than C_L^{mu} for $[Cs]_{liq}$, $[Rb]_{liq}$ and higher for [Ba]liq, electronic supplementary material 2). According to leucogranite phase relations (Scaillet et al., 1995) we should expect that biotite record a higher temperature equilibration stage.

The lack of systematic differentiation from liquids at equilibrium with biotite to liquids at equilibrium with muscovite could find an explanation if the analysed biotites are late in the magmatic history and contemporaneous of muscovite crystallization (e.g. Monier et al 1987; Scaillet et al 2006a). If so, both micas would record identical equilibrium liquids. However, the possibility that biotite is more susceptible than muscovite to late-magmatic trace element reequilibration also needs consideration (Dahl, 1996). Systematic diffusion data to compare the kinetics of trace element reequilibration in biotite and muscovite are presently lacking. Yet, our interpretations of the trace element data suggest that micas in SSLC leucogranites rarely preserve the trace element concentrations of early magmatic liquids.

6.1.2 Pegmatites

Micas in pegmatites exhibit variable Nb/Ta, from > 15 to < 1 (figure 9), the less variable Nb/Ta being for the less fractionated pegmatite (type II). As noted previously for leucogranites, $[Li]_{liq}$ are very homogeneous with Nb/Ta, while $[Cs]_{liq}$, $[Rb]_{liq}$ and $[Ba]_{liq}$ are more variable with Nb/Ta. Liquid compositions for type VI and, to a lesser extent, type V, stand out of the main pegmatite trend on most diagrams (figure 9 and 10). These data points must be considered with caution since they are calculated using partition coefficients for biotite, yet the analysed micas are lepidolites and zinnwaldites.

The evolution of liquid compositions is illustrated in figure 10 and detailed for each pegmatite type separately (electronic Supplementary Material 3). $[Li]_{liq}$ are very similar in most pegmatites, whether calculated from biotite or muscovite. The homogeneous $[Li]_{liq}$ concentrations suggest reequilibration

of mica compositions with a late-magmatic residual melt or fluid. Lepidolite in type VI pegmatite (Chèdeville) has been interpreted as partly magmatic and partly hydrothermal (Raimbault, 1998). If the lepidolite and zinnwaldite data are excluded (see above), micas record $[Li]_{liq}$ between 0.5 and 1.0 wt%, in good agreement with concentrations inferred for pegmatitic melts (Stewart, 1978; Pichavant et al., 1987a; London, 2015). $[F]_{liq}$ concentrations range from ~1 to ~2 wt% (figure 10), also in agreement with estimates for pegmatitic melts (Pichavant and Manning, 1984; Pichavant et al., 1987a; London, 2015). For both Li and F, the maximum concentrations are those calculated from muscovite in type V. Compared to Li, Rb, Ba and Cs demonstrate a larger variability. $[Rb]_{liq}$ and $[Ba]_{liq}$ define correlation respectively positive and negative with $[Cs]_{liq}$, as expected for pegmatite differentiation. However, liquids at equilibrium with biotite are not systematically less evolved than liquids at equilibrium with muscovite. The former are more enriched in Rb, Cs and less enriched in Li, F than the latter. In comparison, muscovites in type V yield the lowest $[Ba]_{liq}$ (the lepidolite and zinnwaldite data being excluded, figure 10).

The pegmatite data strengthen the importance of late-magmatic processes as factors controlling micas compositions. As noted for leucogranites (6.1.1), pegmatites display large variations in Nb/Ta (figure 10). These highly variable ratios are the result of fractionation processes that, for granites, involve biotite and muscovite together (γ_{Go}) or muscovite alone (γ_{Sa}) and, for pegmatites, generally biotite and muscovite together. Based on preliminary mica/melt partition coefficients (constrained from natural occurrences), Stepanov et al. (2014) suggested that biotite and muscovite crystallization can fractionate Nb and Ta. However, in most granites and pegmatites from this study, the fractionating assemblage is the same (biotite plus muscovite), yet only certain samples (the most evolved) strongly fractionate Nb/Ta. This indicates that the Nb/Ta evolution is not governed by the crystallization of micas (e.g. Stepanov et al. 2014). Linnen and Keppler (1997) have demonstrated that, during the evolution of low temperature peraluminous melts, activity coefficients of Ta_2O_5 and Nb_2O_5 are progressively modified. These modifications impact all mineral/melt partition coefficients for Nb and Ta in the same way, always leading to an enrichment of Ta relative to Nb in residual liquids. During the evolution of low temperature peraluminous melts, phases most likely to fractionate Nb from Ta

would include muscovite (Raimbault and Burnol, 1998; Stepanov et al., 2014) and columbo-tantalite (Linnen and Keppler, 1997; Raimbault, 1998; Linnen and Cuney, 2005; Deveaud et al., 2015), which occur respectively in SSLC leucogranites and MAPF pegmatites. The late-magmatic evolution (since both muscovite and columbo-tantalite are late-crystallizing phases) would thus be characterized by the accumulation of Ta relative to Nb as illustrated by muscovite compositions from this study and by the strong Ta/(Ta+Nb) enrichment in columbo-tantalites from the Chèdeville pegmatites (Raimbault, 1998). This magmatic model (compare with the magmatic-hydrothermal model of Ballouard et al., 2016) satisfactorily accounts for the strong Nb/Ta variations observed in both the leucogranites and pegmatites.

6.2 Trace element modelling

6.2.1 Leucogranitic liquids

Given the importance of late-magmatic processes in controlling micas trace element compositions, crystallization models, both reverse and forward, have been constructed to assist in the interpretation of the data. Using Rayleigh's fractional crystallization law, the trace element (i) content of a derivative liquid (C_L^i) can be related to its content in the primary liquid (C_0^i):

(1)

(2) $C_L^i = C_0^i \times F^{(D^i - 1)}$

(3)

where F is the fraction of remaining liquid and D^i the distribution coefficient between liquid and crystallised solids. D^i is determined by the sum of the products of partition coefficients (Kd_n^i, table 1) weighted by the corresponding phase proportions (x_n) according to:

(4)

(5) $D^i = \sum_n x_n \times Kd_n^i$

(6)

Partition coefficients used in the calculations are summarized in table 1 for major phases crystallizing from leucogranitic liquids, which include quartz, alkali feldspar and plagioclase in addition to biotite and muscovite (Scaillet et al., 1995). Phase diagrams for peraluminous leucogranites similar to those of the SSLC enable phase assemblages and proportions to be determined in the crystallization interval from ~800 to ~650°C at 400 MPa (Scaillet et al., 1995). For biotite to crystallize as the sole mica, a residual liquid fraction (*F*) of 45 wt% minimum in needed. Therefore, the calculations assume that biotite in γ_{Br} last equilibrated with a liquid derived from 55 wt% crystallization (*F* = 45 wt%) of the parental melt. Two-mica (biotite-muscovite) phase assemblages require lower *F*, in the range 45 wt% to 0 wt%. In the following, we will assume that biotite and muscovite in two-mica leucogranites last equilibrated with a liquid derived from 80 wt% crystallization (*F* = 20 wt%). For muscovite granite, a *F* value of 10 wt% has been assumed. Note that this assumes that micas compositions are not affected by post-magmatic re-equilibration (i.e. *F* = 0). In another words the modelling aims at testing a reasonable case of late-magmatic crystallisation and trace element reequilibration in micas.

For each leucogranite, the content an element *i* of the original liquid C_0^i can be calculated according to:

(7)

(8) $C_0^i = C_f^i \times F^{(1-D^i)}$

(9)

where *F* is determined as explained above and C_f is the most chemically evolved derivative liquid, obtained from the C_L^{bi} and C_L^{mu} data. Once C_0 is determined, it is then possible, using a forward approach, to establish the evolution of liquid composition from C_0 to C_f by calculating intermediate compositions (C_L) with phase assemblages and proportions from Scaillet et al (1995).

Results of calculations for selected leucogranite types are shown in figure 11, the entire set of calculations being compiled in the electronic Supplementary Material 4. The same principle is applied to pegmatites and presented in figure 12 and electronic Supplementary Material 5. In all cases, calculated C_0 are less evolved i.e., have lower incompatible and higher compatible element concentrations than C_f. For Rb, calculated C_0 - C_L trends reasonably reproduce the $[Rb]_{liq}$ vs. $[Cs]_{liq}$ evolutions in particular for γ_{Sy} and γ_{Sa}. In comparison, the calculated C_0 - C_L values and trends are

systematically lower than the $[Li]_{liq}$ values, especially for γ_{Br} and γ_{Sa} (figure 11). As suggested above, this behaviour can be explained by micas having equilibrated with late residual Li-rich liquids or fluids. Significant differences between measured and modelled liquid concentrations were also noted for Ba. Most C_0 and C_L are higher than $[Ba]_{liq}$ especially for γ_{Br}, γ_{Go} and γ_{Sa} (electronic Supplementary Material 4). C_0 sometimes reach very high concentrations (> 1000 ppm for γ_{Sa}, electronic Supplementary Material 4) which casts doubt on the *Kd* values used in the calculations (table 1). Note that increasing *D* for Ba (to account for the possibility of disequilibrium crystallization, see above) would make C_0 concentrations still higher. Lastly, the apparently incompatible behaviour shown by Ba in γ_{Go} and γ_{Sa} (figure 7) is difficult to explain for magmas crystallizing K-feldspars and suggests hydrothermal mobilisation of Ba, similar to observed for Sr in the Beauvoir granite (Charoy et al., 2003). However, since this study is mainly concerned with incompatible elements, a full understanding of the behaviour of Ba is unwarranted (figure 11).

Whole rock data for leucogranites are compared with simulated trace element evolutions (figure 13a). Whole rocks all plot left (i.e., have lower [Cs]) than their corresponding liquid evolution trends. The whole-rock data for γ_{Sy} and γ_{Ch} plot relatively close to their calculated respective primary melts (C_0) but, for the other granites, the whole-rocks have lower [Rb] and [Li] and, for [Ba], the γ_{Sy} and γ_{Ch} whole-rocks are lower than their corresponding C_0 (figure 13a; electronic supplementary material 4). Therefore, whole-rocks hardly represent liquid compositions. As a consequence, the trends revealed by the whole rock trace element contents (figure 13a) are not the expression of leucogranitic magma differentiation and the use of whole rock trace element contents is not directly relevant to the geochemical evolution of leucogranitic liquids. Liquid compositions exhibit a trace element concentration range considerably wider than whole rocks. Whole-rocks trace element compositions do not reflect the evolution of liquid composition.

6.2.2 Pegmatitic liquids

Although no phase diagram is available for MAPF pegmatites, biotites and muscovites come from intermediate zones mostly composed of K-feldspar and quartz. These zones are viewed as relatively early products of crystallization of the pegmatite leaving a significant volume of residual liquid. Accordingly, we have assumed that intermediate zones derive from 50 wt% crystallization (F = 50 wt%, see above) of the parental liquid. Knowing the mineral assemblage in intermediate zones, the composition of the original liquid can be calculated using equations and partition coefficients as above. Results of calculations for selected pegmatite types are detailed in figure 12 and the entire results are shown in the electronic supplementary material 5.

In type II pegmatite where only biotite was analysed, the calculated Rb and Ba evolutions match reasonably well the C_L^{bi}. Similarly to granites, the liquid evolution calculated for Li yields values much lower than the determined $[Li]_{liq}$ (figure 12), because of equilibration of micas with late Li-rich liquids or fluids. For the other pegmatite types, the C_L^{bi} and C_L^{mu} data points cannot be reconstructed starting from a single most chemically evolved derivative liquid C_f (figure 12; electronic supplementary material 5). For example, the evolution for the type III pegmatite calculated from the most evolved biotite generates liquids with Rb concentrations still higher than those derived from muscovite (figure 12). As noted previously, in type III pegmatite, muscovites record higher $[Rb]_{liq}$ and $[Cs]_{liq}$ and equal or lower $[Li]_{liq}$, $[Ba]_{liq}$ and $[F]_{liq}$ than biotites. The difference between liquids derived from biotite and muscovite is especially marked for Cs, and biotite can record liquid Cs concentrations up 10 times higher than muscovite (see for example type III, figure 12). Consequently, for most pegmatites, the calculations are divided in two parts, one starting from C_f constrained from biotite and the other from C_f constrained from muscovite (figure 12; electronic supplementary material 5). These differences between muscovite and biotite are attributed to specific crystallization environments for biotite and muscovite in the same pegmatite. Studies of the Chèdeville pegmatites have demonstrated that they crystallized from several separate melt pulses instead of from a single batch (Raimbault, 1998). Consequently, the biotites and muscovites analysed are not necessarily comagmatic. Nevertheless, their compositions can inform on the range of primary melts as well as on trace element evolutions during crystallization. Results of the modelling generate primary melt compositions (C_0) that stay

relatively close to the determined C_L^{bi} and C_L^{bi} data (figure 12; electronic supplementary material 5). For Rb in type III, IV and V, the calculated evolutions reproduce quite well the biotite and muscovite data. For Ba and Li, the fits are less good and variable between mica and pegmatite types. It is possible that some pegmatites bear the mark of late-magmatic fluid-dominated processes as indicated by the crystallization of lepidolite and zinnwaldite instead of biotite in type VI pegmatite (Raimbault, 1998). Whole rocks compositions for lepidolite and aplite units in type VI (Chèdeville) are compared to calculated liquid contents in figure 13b. [Cs] contents of lepidolite and aplite units from type VI (table 3) match the lowest $[Cs]_{liq}$ (figure 13b, electronic supplementary material 6). [Li] and [Ba] from whole rocks are similar to that of liquids, and [Rb] are significantly higher in whole rocks than in liquids from other pegmatite types (figure 13b, electronic supplementary material 6).

6.3 The granite-pegmatite connection

The mutual relations between leucogranites, pegmatites and leucogranites and pegmatites are explored on figure 13. No derivative liquid (C_f) from the crystallization of one leucogranite matches the composition of the primary liquid (C_0) for another leucogranite. Thus, no geochemical continuity exists from one leucogranite to the other. γ_{Br}, γ_{Go} and γ_{Sa} plot on the same evolution line for $[Li]_{liq}$ (electronic supplementary material 6) but this is not the case for $[Rb]_{liq}$ (figure 13c) and, so, these various leucogranite phases cannot be related to each other by fractional crystallization (Deniel et al 1987; Guillot and Le Fort, 1995). Similarly, compositions of primary liquids in pegmatites and trace element evolutions do not plot in continuity with each other (figure 13c). Differences also exist between liquids calculated from biotite and from muscovite in the same pegmatite (electronic supplementary material 6). Compositions of primary granitic and pegmatitic liquids overlap, the less evolved of the range being represented by γ_{Sy} and the most evolved by liquids for the type V pegmatite. Primary liquids for leucogranites can be more evolved than for pegmatites (e.g., γ_{Sa}) and the reverse is also true. Several primary pegmatitic liquids are more evolved than residual leucogranitic liquids (C_f). Therefore, despite uncertainties in the modelling (partition coefficients and *F* estimations,

see above), no systematic relation emerges between compositions of granitic and pegmatitic melts (such as, for example, pegmatitic being systematically more evolved than granitic melts). The data and the modelling are consistent with each liquid evolving independently from the others. This implies that both pegmatite and granite melts are differentiated from their origin (i.e., different C_0). Differentiation is thus inherited from source processes rather than being the consequence of fractional crystallization of a single parental magma.

In addition, the model above, which emphasizes similarities between granitic and pegmatitic melts, raises the question of the origin of textural differences between granites and pegmatites in the SSLC and the MAPF. Previous studies have suggested that these textural differences could be the consequence of:

1. Differences in volatile concentrations (H_2O, F, B) between melts at the origin of granites and pegmatites. In particular, the possibility of very high H_2O contents (> 10 wt.%) in pegmatitic melts has been suggested by Thomas et al. (2010).
2. Different emplacement dynamics and volumes for granitic and pegmatitic melts leading to contrasted cooling and crystallization regimes promoting the development of specific textures (Lofgren, 1974 and 1980; London, 1992).

On the first point, our data show that the $[F]_{liq}$ and $[Li]_{liq}$ concentrations do not largely differ between leucogranitic and pegmatitic liquids. For example, $[F]_{liq}$ at equilibrium with muscovite in γ_{Sa} (1 - 2 wt.% figure 7) are in the same range than $[F]_{liq}$ for most pegmatites (except in type V and also type VI if the lepidolite and zinnwaldite data are considered, table 4). Thus, neither $[F]_{liq}$ nor $[Li]_{liq}$ contents can account for the textural differences observed between granite and pegmatite. In addition, experimental H_2O contents in pegmatitic melts containing F, B, Li and P are higher than in melts devoid of these components but solubilities never exceed 10 wt.% H_2O below 3 kbar (Holtz et al., 1993; Bartels et al., 2011). Therefore, differences in volatile concentrations between respective melts do not appear sufficient to explain the textural differences between granite and pegmatite. We suggest that pegmatites in the MAPF originate from similar processes than SSLC granites but, as melt

compositions were essentially similar, pegmatitic textures developed as a consequence of specific magma volumes; emplacement dynamics; crystallisation and cooling regimes.

6.4 Processes controlling magmatic differentiation

The similarities documented above between granitic and pegmatitic melts suggest that they have undergone a similar evolution and so that pegmatites from the MAPF can hardly be considered as fractionation products from the SSLC granitic magmas. According to our reconstructed liquid compositions, the differentiation observed among SSLC granites and MAPF pegmatites does not occur "on site", but prior to emplacement. In this case, magmatic differentiation could alternatively take place either in the source region or during magma transport on its way to the emplacement site. Previous studies of the SSLC have pointed out the proximity of the granite to its probable source in the Lower Gneiss Unit (e.g. Turpin et al 1990). This implies that magma transport would take place over relatively short distances. There is also no evidence for the presence of intermediate granitic bodies between the source rock level and the SSLC. In that sense, the geochemical variability within SSLC granites and MAPF pegmatites would be most probably related to source processes. The relative geochronological relationships between each granite facies (Friedrich, 1984; Cuney et al. 2002) support assembly of the SSLC from different but compositionally similar magma batches generated from the same source area in the crust. Equilibrium melting of a single source coupled to discrete episodes of melt extraction could lead to elemental fractionations within the source region. The observed differentiation between the different magma batches could thus be the result of various processes including:

1. Variable degrees of melting. For example, decreasing melting rates would enrich incompatible element concentrations in the melt. It is possible that early-formed magmas are produced through larger melt fractions and are thus less enriched than late formed magmas originating from residual source (Wolf et al., 2018). A progressive decrease in melting rate with time could be the consequence of previous melt extraction reducing source fertility.

2. Near-source prograde crystallization of quartz and feldspars (e.g. Nicoli et al 2017). Such processes would have geochemical implications (i.e., increased fractionation) similar to those proposed by Tartese et al (2010) although, in this case, these would occur within or near the migmatitic area.
3. Disequilibrium melting (Nabelek and Glascock, 1995; Villaros et al 2009; McLeod et al 2012) allowing the retention of incompatible elements during the earlier stages of melting. In this case, rare metals would remain “trapped” in the source and only progressively “released” in the melt.
4. Melting affecting progressively different layers of a heterogeneously enriched source. Romer et al. (2014) have suggested that the source of rare metal granite magmas can be anomalously and heterogeneously enriched as a consequence of previous sedimentary processes. In the Variscan Orogen, such a model is supported by the location of rare metals magmas.

Combinations of all the above processes would account for the differentiation observed in granite but also in pegmatite melts and, in particular, for the differential initial rare metal enrichments observed in the granitic and pegmatitic bodies.

7 Conclusions

The approach used here appears to be fruitful for reconstituting the evolution of parental liquids. Despite (partial) equilibrations of micas and uncertainties over partition coefficients, micas record, at least partly, the evolution of granitic and pegmatitic liquid composition. The reconstruction of trace element contents of granitic and pegmatitic liquids from the analysis of mica compositions demonstrate that 1) the SSLC granites and the MAPF pegmatite do not simulate a liquid line of descent and, thus, that granitic magmas are not parental to pegmatitic melts. Both granites and pegmatites have a common origin and exhibit different levels of fractionation as a consequence of mainly source processes. 2) Liquid fractionation recorded by biotite and muscovite occurs during the

internal differentiation of each igneous body, which includes the effects of crystallization of major and accessory mineral phases and also the involvement of late-magmatic fluids.

Finally, we stress that whole rock compositions can hardly be used directly to reconstruct the magmatic evolution that leads to granite. These merely provide a qualitative record of the entire process. The use of mineral composition and melt/mineral partition as presented here appears considerably more promising than whole rock compositions studies. It provides a semi-quantitative estimate of melt trace elements contents during crystallization. Further use of this approach requires caution as mineral/melt partitions uncertainties and the effect of equilibration over each element must be considered. Ultimately, the determination of melt composition would benefit additional studies of mineral/melt partitioning and trace element diffusion in micas (and other minerals).

Acknowledgements

The authors acknowledge funding from Labex VOLTAIRE (ANR-10-LABX-100-01) and the ANR project VARPEG. Sarah Deveaud is thanked for her participation to the analysis of micas from pegmatites. Thanks to Don Dingwell for handling of the manuscript and to anonymous reviewers for their suggestions that helped improving this manuscript.

References

Abdel-Rahman, A.F.M., 1994. Nature of biotites from alkaline, calc-alkaline, and peraluminous magmas. *J. Petrol.*, ***35***(2), 525-541.

Aréne, J., Autran, D., Cofrant, H., Labernadiere, L., Burnol, L., 1979. Feuille de Bourganeuf, Carte géologique de France 1/50000 **665**. BRGM, Paris.

Audrain, J., Vigneresse, J.L., Cuney, M., Friedrich, M., 1989. Modèle gravimétrique et mise en place du complexe granitique hyperalumineux de Saint-Sylvestre (Massif Central français). *C. R. Acad. Sci. Sér. 2 Méca. Phys. Chim. Sci. Univers Sci. Terre* **309**, 1907–1914.

Ballouard, C., Poujol, M., Boulvais, P., Branquet, Y., Tartese R., Vigneresse J.-L., 2016. Nb-Ta fractionation in peraluminous granites: A marker of the magmatic hydrothermal transition. *Geology*. **44**, 231-234.

Bartels, A., Vetere, F., Holtz, F., Behrens, H., Linnen, R.L., 2011. Viscosity of flux-rich pegmatitic melts. *Contrib. Mineral. Petrol.* **162**, 51–60.

Bea, F., Pereira, M.D., Corretgé, L.G. and Fershtater, G.B., 1994. Differentiation of strongly peraluminous, perphosphorus granites: The Pedrobernardo pluton, central Spain. *Geochim. Cosmochim. Acta*. **58**, 2609-2627.

Breiter, K., Fryda, J., Seltmann, R., Thomas, R., 1997. Mineralogical evidence for two magmatic stages in the evolution of an extremely fractionated P-rich rare-metal granite: the Podlesi Stock, Krusne Hory, Czech Republic. *J. Petrol*. **38**, 1723–1739.

Bucholz, C.E., Stolper, E.M., Eiler, J.M., & Breaks, F.W., 2018. A Comparison of Oxygen Fugacities of Strongly Peraluminous Granites across the Archean–Proterozoic Boundary. *J Petrol*, **59**, 2123-2156.

Cathelineau, M., Boiron, M.C., Holliger, P., Poty, B., 1990. Metallogenesis of the French part of the Variscan ororgeny. Part II: Time-space relationships between U, Au, Sn, W ore deposition and geodynamic events- mineralogical and U/Pb data. *Tectonophysics* **177**, 59–79.

Černý, P., 1991. Rare-element granitic pegmatites. Part I anatomy and internal evolution of pegmatites deposits. *Geosci. Can.* **18**, 49-67.

Černý, P., Ercit, T.S., 2005. The classification of granitic pegmatites revisited. *Can. Mineral.* **43**, 2005-2026.

Charoy, B., Noronha, F., 1996. Multistage growth of a rare-element, volatile-rich microgranite at Argemela (Portugal). *J. Petrol.* **37**, 73-94.

Charoy, B., Chaussidon, M., Le Carlier de Veslud, C., Duthou, J.L., 2003. Evidence of Sr mobility in and around the albite-lepidolite-topaz granite of Beauvoir (France): an in-situ ion and electron probe study of secondary Sr-rich phosphates. *Contrib. Mineral. Petrol*. **145**, 673-690.

Cheilletz, A., Cuney, M., Charoy, B., Archibald, D.A., 1992. ^{40}Ar/^{39}Ar dating of topaz-lepidolite Beauvoir leucogranite and Chèdeville sodium-lithium pegmatites (North Massif Central, France); Petrological and geodynamical meaning. *C. R. Acad. Sci. Paris* **315**, 326-336.

Cherniak, D.J., 2010. Cation Diffusion in Feldspars. *Rev Mineral* **72**, 691-733.

Cuney, M., Friedrich, M., Blumenfeld, P., Bourguignon, A., Boiron, M.-C., Vigneresse, J.-L., Poty, B., 1990. Metallogenesis in the French part of the Variscan Orgogen. Part I: U préconcentrations in the pre-Variscan and Variscan formations – A comparison with Sn, W and Au. In: Ph. Matte (Ed), Terranes in the Variscan Belt of Europe and Circum Atlantic Paleozoic Orogens. *Tectonophysics*, **177**, 39-57.

Cuney, M., Marignac, C., Weisbrod, A., 1992. The Beauvoir topaz-lepidolite albite granite (Massif Central, France); the disseminated magmatic Sn-Li-Ta-Nb-Be mineralization. *Econ. Geol.* **87**, 1766-1794.

Cuney, M., Alexandrov, P., Le Carlier de Veslud C., Cheilletz A., Raimbault L., Ruffet G., Scaillet S., 2002. The timing of W-Sn rare metals mineral deposit formation in the Western Variscan chain in their orogenic setting : the case of the Limousin area (Massif Central, France). *Geol. Soc. Lond. Spec. Publ.* **204**, 213-228.

Czamanske, G.K., Wones, D.R., 1973. Oxidation During Magmatic Differentiation, Finnmarka Complex, Oslo Area, Norway: Part 2, The Mafic Silicates1. *J. Petrol.*, **14(3)**, 349-380.

Dahl, P.S., 1996. The crystal-chemical basis for Ar retention in micas: inferences from interlayer partitioning and implications for geochronology. *Contrib. Mineral. Petrol*. **123**, 22-39.

Debon, F., Le Fort P., 1983. A chemical–mineralogical classification of common plutonic rocks and associations. T. Roy. Soc. Edin-Earth, **73**, 135-149.

Deniel, C., Vidal, P., Fernandez, A., Le Fort, P., Peucat, J. J., 1987. Isotopic study of the Manaslu granite (Himalaya, Nepal): inferences on the age and source of Himalayan leucogranites. *Contrib. Mineral. Petrol.*, **96**, 78-92.

Deveaud, S., Gumiaux, C., Gloaguen, E., Branquet, Y., 2013. Spatial statistical analysis applied to rare-element LCT-type pegmatite fields: an original approach to constrain faults-pegmatites-granites relationships. *J. Geosci.* **58**, 163–182.

Deveaud, S., Millot, R., Villaros, A., 2015. The genesis of LCT-type granitic pegmatites, as illustrated by Lithium isotopes in micas. *Chem. Geol.*. **411**, 97-111.

Faure, M., Lardeaux, J.-M., Ledru, P., 2009. A review of the pre-Permian geology of the Variscan French Massif Central. *C. R. Geosci.* **341**, 202-213.

Faure, M., Pons, J., 1991. Crustal thinning recorded by the shape of the Namurian-Westphalian leucogranite in the Variscan belt of the northwest Massif Central, France. *Geology* **19**, 730–733.

Floc'h, J., 1983. A travers une branche de la Chaîne Varisque, depuis l'Aquitaine à la zone d'Argentat (Massif Central, France). (Sciences de la Terre). Thèse de Doctorat, Univ. Limoges

Freidrich, M., 1984. Le complexe granitique hyperalumineux de Saint Sylvestre, Nord-Ouest du Massif Central Français. Thèse INPL Nancy, Géologie et Géochimie de l'Uranium mem n°5.

Friedrich, M., Cuney, M., Poty, B., 1987. Uranium geochemistry in peraluminous granites. *Uranium* **3**, 353-385.

Guillot, S., Le Fort, P., 1995. Geochemical constraints on the bimodal origin of High Himalayan leucogranites. *Lithos*, **35**, 221-234

Goodenough, K.M., Lusty, P.A.J., Roberts, N.M.W., Key, R.M., Garba, A., 2014. Post-collisional Pan-African granitoids and rare metal pegmatites in western Nigeria: Age, petrogenesis, and the 'pegmatite conundrum'. *Lithos*, **200-201**, 22-34.

Hammouda, T., Cherniak, D.J., 2000. Diffusion of Sr in fluorphlogopite determined by Rutherford backscattering spectrometry, *Earth Planet. Sci. Lett.* **178**, 339-349.

Hanson, G.N., 1978. The application of trace elements to the petrogenesis of igneous rocks of granitic composition. *Earth Planet. Sci. Lett.* **38**, 26-43.

Hoffman, A.W., Giletti, B.J., 1970. Diffusion of geochronologically important nuclides in minerals under hydrothermal conditions, *Eclog. Geolog. Helvet.*, **63**, 141-150

Holliger, P., Cuney, M., Friedrich, M., Turpin, L., 1986. Age carbonifère de l'unité de Brame du complexe granitique peralumineux de Saint-Sylvestre (N.O. Massif Central) définit par les données isotopiques U-Pb sur zircon et monazite. *C. R. Acad. Sci. Sér. 2 Mécanique Phys. Chim. Sci. Univers Sci. Terre* **303**, 1309–1314.

Holtz, F., Dingwell, D. B., Behrens, H., 1993. Effects of F, B_2O_3 and P_20_5 on the solubility of water in haplogranite melts compared to natural silicate melts. *Contrib. Mineral. Petrol.* **113**, 492-501.

Hottin, A., Delbos, R., Pellaton, C., Depuis, J., Usnarki, G., Marchiol, A., Vecsei, A., 1995. Feuille de Magnac-Laval (640). Carte géologique de France 1/50000. BRGM, Paris.

Hulsbosch N., Hertogen J., Dewaele S., André L., Muchez Ph., 2014. Alkali metal and rare earth element evolution of rock-forming minerals from the Gatumba area pegmatites (Rwanda): Quantitative assessment of crystal-melt fractionation in the regional zonation of pegmatite groups. *Geochim. Cosmochim. Acta*, **132**, 349-374.

Icenhower, J., London, D., 1995. An experimental study of element partitioning among biotite, muscovite, and coexisting peraluminous silicic melt at 200 MPa (H_2O). *Amer. Mineral.* **80**, 1229–1251.

Icenhower, J., London, D., 1996. Experimental partitioning of Rb, Cs, Sr, and Ba between alkali feldspar and peraluminous melt. *Am. Mineral.* **81**, 719–734.

Jahns, R.H., Burnham, C.W., 1969. Experimental studies of pegmatite genesis. I. A model for the derivation and crystallization of granitic pegmatites. *Econ. Geol.* **64**, 843-864.

Kontak, D. J., 2006. Nature and origin of an LCT-suite pegmatite with late-stage sodium enrichment, Brazil Lake, Yarmouth County, Nova Scotia. I. Geological setting and petrology. *Can. Mineral.* **44**, 563-598.

Kaeter, D., Barros, R., Menuge, J. F., Chew D.M., 2018. The magmatic–hydrothermal transition in rare-element pegmatites from southeast Ireland: LA-ICP-MS chemical mapping of muscovite and columbite–tantalite. *Geochimica et Cosmochimica Acta*, **240,** 98-130.

Legros, H., Marignac, C., Tabary, T., Mercadier, J., Richard, A., Cuney, M., Wang, R-C., Charles, N., and Lespinasse, M.Y., 2018. The ore-forming magmatic-hydrothermal system of the Piaotang W-Sn deposit (Jiangxi, China) as seen from Li-mica geochemistry. *American Mineralogist*, **103**, 39-54.

Leroy, J., 1978. The Margnac and Fanay Uranium deposits of the La Crouzille District (Western Massif Central, France) : Geologic and fluid inclusion studies. *Econ. Geol.* **73**, 1611-1634.

Lespinasse, M., Cathelineau, M., (1990) Fluid percolations in a fault zone: a study of fluid inclusion planes in the St Sylvestre granite, northwest Massif Central, France. *Tectonophysics* **184**, 173-187.

Le Carlier Le Veslud, C., Alexandre, P., Ruffet, G., Cuney, M., Cheilletz, A., 2013. A two-stage exhumation in Western French Massif Central: New geochronological evidences of syn-collisional extension. *Lithos* **175–176**, 1–15.

Linnen, R.L., Cuney, M., 2005. Granite-related rare-element deposits and experimental constraints on Ta-Nb-W-Sn-Zr-Hf mineralization. In Linnen, R.L. and Samson, I.M., eds., Rare-Element Geochemistry and Mineral Deposits: Geolog. Assoc. Canada, GAC Short Course Notes **17**, p. 45-67.

Linnen, R.L., Keppler, H., 1997. Columbite solubility in granitic melts: consequences for the enrichment and fractionation of Nb and Ta in the Earth's crust. *Contrib. Mineral. Petrol*. **128**, 213-227.

Lofgren, G.E., 1974. An experimental study of plagioclase crystal morphology: isothermal crystallization. *Amer. J. Sci* **274**, 243-273.

Lofgren, G.E., 1980. Experimental studies on the dynamic crystallization of silicate melts. In *Physics of Magmatic Processes*, R. B. Hargraves, ed. Princeton University Press, Princeton, New Jersey, 487-551.

London, D., 1992. The application of experimental petrology to the genesis and crystallization of granitic pegmatites. *Can. Mineral.*, **30**, 499-540

London, D., 2005. Granitic pegmatites: an assessment of current concepts and directions for the future. *Lithos*. **80**, 281-303.

London, D., 2009. The origin of primary textures in granitic pegmatites. *Can. Mineral.* **47**, 697–724.

London, D., 2014. A petrologic assessment of internal zonation in granitic pegmatites. *Lithos*. **184-187**, 74-104.

London D., 2015. Reply to Thomas and Davidson on "A petrologic assessment of internal zonation in granitic pegmatites" (London, 2014a). *Lithos* **212-215**, 469-484.

London, D., Morgan, G.B.VI, 2012. The pegmatite puzzle. Elements, 8, 263-268.

Marignac, C., Cuney, M., 1999. Ore deposits of the French Massif Central : insight into the metallogenesis of the Variscan collision belt. *Miner. Deposita* **34**, 472-504.

McCarthy, T.S., Groves D.I., 1979. The Blue Tier batholith, northeastern Tasmania - A cumulate-like product of fractional crystallization. *Contrib. Mineral. Petrol.* **71**, 193-209.

McIntire, W.L., 1963. Trace element partition coefficients – a review of theory and applications to geology. *Geochim. Cosmochim. Acta.* 27, 1209-1264.

McLeod, C., Davidson, J.P., Nowell, G.M., de Silva Shanaka, L., 2012. Disequilibrium melting during crustal anatexis and implications for modeling open magmatic systems. *Geology.* **40**, 435-438.

Melleton, J., Gloaguen, E., Frei, D., Novak, M. and Breiter, K., 2012. How Are the Emplacement of Rare-Element Pegmatites, Regional Metamorphism and Magmatism Interrelated in the Moldanubian Domain of the Variscan Bohemian Massif, Czech Republic? *Can. Mineral.* **50**, 1751–1773.

Melleton, J, Gloaguen, E., Frei, D., 2015. August. Rare-elements (Li-Be-Ta-Sn-Nb) magmatism in the European Variscan belt, a review. In SGA 2015 *807-810*

Michallik, R.M., Wagner, T., Fusswinkel, T., Hzinonen, J.S., Heikkila, P., 2017. Chemical evolution and origin of the luumäki gem beryl pegmatite: Constraints from mineral trace element chemistry and fractionation modeling. Lithos. 274-275, 147-168.

Miller, C.F., Stoddard E.,F., Bradfish, L.J., Dollase, W.A., 1981. Composition of plutonic muscovite: genetic implications. *Can Mineral.* **19**, 25-34.

Mollier, B., 1984. Le Granite de Brame-St Sylvestre-St Goussaud: ses structures magmatiques; une étude de la distribution de l'uranium à l'échelle du grain Thèse de doctorat, CReGU, Nancy Univ. 251p

Mollier, M., Bouchez J.-L., 1982. Structuration magmatique du complexe granitique de Brame-St Sylvestre-St Goussaud (Limousin, Massif Central Français) *C. R. Acad. Sci., Ser. 2.* **294**, 1329–1333.

Mollier, B., Lespinasse, M., 1985. Déformation magmatique et plastique en limite Nord du granite de Saint-Sylvestre (Nord-Ouest du Massif Central français): la faille d'Arênes-Ouzilly. *C. R. Acad. Sci. Sér. 2 Mécanique Phys. Chim. Sci. Univers Sci. Terre* **300**, 681–696.

Monier, G., 1987. Cristallochimie des micas des leucogranites: nouvelles données expérimentales et applications pétrologiques. Thèse de doctorat, CReGU, Nancy, Univ. 264.

Monier, G., Charoy, B., Cuney, M., Ohnenstetter, D., Robert, J-L. 1987. Evolution spatiale et temporelle de la composition des micas du granite albitique à topaze-lépidolite de Beauvoir. *Géol. France*, **2-3**, 179-188.

Monier, G., Robert, J.L., (1986). Muscovite solid solutions in the system K_2O-MgO-FeO-Al_2O_3-SiO_2-H_2O: an experimental study at 2 kbar PH_2O and comparison with natural Li-free white micas. *Mineral. Mag*, **50**, 257-266.

Morgan, G.B.VI., London, D., 2003. Trace-element partitioning at conditions far from equilibrium: Ba and Cs distributions between alkali feldspar and undercooled hydrous granitic liquid at 200 MPa. *Contrib. Mineral. Petrol.*, **144**, 722-738.

Müller, A., Seltmann, R., Halls, C., Siebel, W., Dulski, P., Jeffries, T., Spratt, J., Kronz, A., 2006. The magmatic evolution of the Land's End pluton, Cornwall, and associated pre-enrichment of metals. *Ore Geol. Rev.* **28**, 329–367.

Nabelek, P.I., Russ-Nabelek, C., Denison, J.R., 1992a. The generation and crystallization conditions of the Proterozoic Harney Peak leucogranite, Black Hills, South Dakota. *Contrib. Mineral. Petrol.*, **110**, 173-191.

Nabelek, P.I., Russ-Nabelek, C., Haeussler, G.T., 1992b. Stable isotope evidence for the petrogenesis and fluid evolution in the Proterozoic Harney Peak leucogranite, Black Hills, South Dakota. *Geochim. Cosmochim. Acta,* **56**, 403-417.

Nabelek, P.I., Glascock M.D., 1995. REE-Depleted leucogranites, Black Hills, South Dakota: a consequence of disequilibrium melting of monazite-bearing Schists. *J. Petrol.* **36**, 1035-1071.

Nachit H. (1985). Composition chimique des biotites et typologie magmatique des granitoids. *C R Hebdom Acad Sci*, **301**, 813-818.

Nash, W., Crecraft, H., 1985. Partition coefficients for trace elements in silicic magmas *Geochim. Cosmochim. Acta,* **49**, 2309-2322

Nicoli, G., Stevens, G., Moyen, J.-F., Vezinet, A., Mayne, M., 2017. Insights into the complexity of crustal differentiation: K_2O-poor leucosomes within metasedimentary migmatites from the Southern Marginal Zone of the Limpopo Belt, South Africa Journal of Metamorphic Geology, in press.

Patureau, J., 1982. Etude des pegmatites des Monts d'Ambazac (Margnac, Le Mas Barbu), (Haute-Vienne). Thèse de doctorat, Université Paul Sabatier, Toulouse, 243.

Pearce, N.J.G., Perkins, W.T., Westgate, J.A., Gorton, M.P., Jackson, S.E. Neal, C.R., Chenery, S.P., 1997. A compilation of new and published major and trace element data for NIST SRM 610 and NIST SRM 612 glass reference materials. *Geostand. Geoanal. Res.* **21**, 115-144

Pichavant, M., Manning, D.A.C., 1984. Petrogenesis of tourmaline granites and topaz granites; the contribution of experimental data. *Phys. Earth Planet. Int*., **35**, 31-50.

Pichavant, M., Herrera, J.V., Boulmier S., Briqueu L., Joron J.-L., Juteau M., Marin L., Michard A., Sheppard S.M.F., Treuil M., Vernet M. 1987a. The Macusani glasses SE Peru: evidence of chemical fractionation in peraluminous magmas. Geochem. Soc. Sp. Pub. **1**, 359-374.

Pichavant, M., Boher, M., Stenger, J.-F., Aïssa, M., Charoy, B., 1987b. Relations de phases des granites de Beauvoir entre 1 et 3 kbar en conditions de saturation en H2O. *Géol. Fr*., **2-3**, 77-85.

Pichavant, M., Villaros, A., Deveaud, S., Scaillet, B., Lahlafi M., (2016) Influence of redox state on mica crystallization in leucogranitic and pegmatitic liquids. *Can. Mineral.* **54**, 559-581.

Pollard, P., Pichavant, M., Charoy, B., 1987. Contrasting evolution of fluorine-rich and boron-rich tin systems. *Miner. Dep*. **22**, 315-321.

Raimbault, L., 1998. Composition of complex lepidolite-type granitic pegmatites and of constituent columbite-tantalite, Chedeville, Massif Central, France. *Can. Mineral.* **36**, 563–583.

Raimbault, L., Burnol, L., 1998. The Richemont rhyolite dyke, Massif Central France: a subvolcanic equivalent of rare-metal granites. *Can. Mineral*. **36**, 265-282.

Raimbault, L., Meyer, G., Treuil, M., 1987. Comportements différenciés de W, Sn, U, Ta, Nb dans quelques complexes granitiques du Massif Central français. *Bull. Mineral.* **110**, 591-601.

Raimbault, L., Cuney, M., Azencott, C., Duthou, J.-L., Joron J.-L., 1995. Geochemical evidence for a multistage magmatic genesis of Ta-Sn-Li mineralization in the granite at Beauvoir, French Massif Central. *Econ Geol* **90**, 548-576.

Roda-Robles, E., Pesquera, A., Velasco, F., Fontan, F., 1999. The granitic pegmatites of the Fregeneda area (Salamanca, Spain) Characteristics and petrogenesis. *Mineral. Mag.*, **63**, 535-556.

Romer, R.L., Meixner, A., Förster, H.-J., 2014. Lithium and boron in late-orogenic granites. Isotopic fingerprints for the source of crustal melts ? *Geochim. Cosmochim. Acta* **131**, 98-114.

Shaw, D.M., 2006. Trace Elements in Magmas: A Theoretical Treatment. Cambridge University Press, 243 p.

Scaillet, B., Pichavant, M., Roux, J., 1995. Experimental crystallization of leucogranite magmas. *J. Petrol.* **36**, 663-705

Scaillet, S., Cheilletz, A., Cuney, M., Farrar, E., Archibald, D.A., 1996. Cooling pattern and mineralization history of the Saint Sylvestre and western Marche leucogranite pluton, French Massif Central: I. $^{40}Ar/^{39}Ar$ isotopic constraints. *Geochim. Cosmochim. Acta* **60**, 4653–4671.

Simmons, W.B., Foord, E.E., Falster, A.U., King, V.T., 1995. Evidence for an anatectic origin of granitic pegmatites, Western Maine, USA. *Geol. Soc. Amer. Ann. Mtng., New Orleans, LA, Abstr. Prog.*, **27**, A411.

Simmons, W.B., Foord, E.E., Falster, A.U., 1996. Anatectic origin of granitic pegmatites, *Western Maine, USA. GAC-MAC Ann. Mtng., Winnipeg, Abstr. Prog*., A87.

Simmons, W.B., Webber, K.L., 2008. Pegmatite genesis: state of the art. *Eur. J. Mineral.* **20**, 421-438.

Sirbescu, M.-L., Nabelek P.I., 2003. Crustal melts below 400 degrees C. *Geology* **31**, 685-688.

Stepanov, A., Hermann, J., 2013. Fractionation of Nb and Ta by biotite and phengite: implications for "missing Nb paradox". *Geology*, **41**, 303-306.

Stepanov, A., Mavrogenes, J.A., Meffre, S., Davidson, P.,2014. The key role of mica during igneous concentration of tantalum. *Contrib. Mineral. Petrol.* **167**, 1001-1009.

Stewart, D.B., 1978. Petrogenesis of lithium-rich pegmatites. *Am. Mineral*. **63**, 970-980.

Tartese, R., Boulvais, P., 2010. Differentiation of peraluminous leucogranites "en route" to the surface. *Lithos* **114**. 353-368.

Thomas, R., Davidson, P., 2012. Water in granite and pegmatite-forming melts. *Ore Geol. Rev.* **46**, 32-46.

Tischendorf, G., Gottesmann, B., Foerster, H.J., Trumbull, R.B., 1997. On Li-bearing micas; estimating Li from electron microprobe analyses and an improved diagram for graphical representation. *Mineral. Mag*. **61**, 809–834.

Treuil, M., Joron, J.-L., 1975. Utilisation des éléments hygromagmatophiles pour la simplification de la modélisation quantitative des processus magmatiques. Exemples de l'Afar et de la dorsale médioatlantique. *Società Italania Mineralogia e Petrologia*, **XXXI**, 125-174.

Turpin, L., Cuney, M., Friedrich M., Bouchez, J.-L., Aubertin, M., 1990. Meta-igneous origin of Hercynian peraluminous granites in N-W French Massif Central : implications for crustal history reconstructions. *Contrib. Mineral. Petrol.* **104**, 163-172.

Van Lichtervelde, M., Holtz F., Melcher, F., 2018. The effect of disequilibrium crystallization on Nb-Ta fractionation in pegmatites: Constraints from crystallization experiments of tantalite-tapiolite. *Amer. Mineral.*, **103**, 1401-1416.

Vidal, P., Bernard-Griffiths, J., Cocherie, A., Le Fort, P., Peucat, J.J., Sheppard, S.M.F., 1984. Geochemical comparison between Himalayan and Hercynian leucogranites. *Phys. Earth Planet. Inter.* **35**, 179–190.

Villaros, A., Stevens G., Buick, I.S., Moyen, J.-F., 2009. The trace element compositions of S-type granites: evidence for disequilibrium melting and accessory phase entrainment in the source. *Contrib. Mineral. Petrol.* **158**, 543–561.Wolf, M., Romer, R.L., Franz, L., López-Moro, F.J., 2018. Tin in granitic melts: The role of melting temperature and protolith composition. Lithos. **310-311**, 20-30.

Wones, D. R., Eugster, H.P., 1965. Stability of biotite: Experiment, theory, and application: *Amer. Mineral*, **50**, 1228-1272.

Webster, J. D., Thomas, R., Rhede, D., Förster, H.-J., Seltmann R., 1997. Melt inclusions in quartz from an evolved peraluminous pegmatite: Geochemical evidence for strong tin enrichment in fluorine-rich and phosphorus-rich residual liquids. *Geochim Cosmochim Acta* **61**, 2589-2604.

Zhang, Y., Ni, H., Chen, Y., 2010. Diffusion Data in Silicate Melts. Reviews in Mineralogy and Geochemistry, 2010, 72, 311-408.

Zhu, Z., Wang, R., Marignac, C., Cuney, M., Mercadier, J., Che, X., Lespinasse, M.-Y., 2018. A new style of rare metal granite with Nb-rich mica: The Early Cretaceous Huangshan rare-metal granite suite, northeast Jiangxi Province, southeast China. *Amer Mineral*, **103**, 1530-1544.

Figure captions

Figure 1. Schematic theoretical evolution of two highly incompatible elements (*i* and *j*) in liquids in the case of fractional crystallization of cogenetic liquids (left) and fractional crystallization of non-cogenetic liquids generated by discrete episodes of partial melting (right). Liquid composition progressively varies between the initial composition (C_0) and the final liquid composition (C_f). The crystallization of liquids intermediate between C_0 and C_f yields granite and pegmatite magmas (M_1, M_2, M_3 and M_4) with different mineral assemblages, proportions and incompatible element enrichments. In the case of fractional crystallization of cogenetic liquids, a single linear trend is observed between liquids and, in principle, between magmas. On the contrary, in the case of fractional crystallization of non-cogenetic liquids, independent liquid and magma evolutionary trends are obtained. See also Treuil et Joron (1975), Raimbault et al. (1987) and Shaw (2006).

Figure 2. Experimentally determined mica/melt partition coefficients (Kd = concentration of trace element i in mica/ concentration of trace element *i* in melt) for biotite (bi) and muscovite (mu) and Rb, Ba, Cs, Be, Li and F plotted as a function of temperature (between 600 and 800 °C. Data are from Icenhower and London (1995) and Pichavant et al. (2016). Minimum and maximum values are defined as explained in text (grey dashed and solid lines for biotite/liquid and muscovite/liquid respectively). Preferred values are defined arbitrarily (black dashed and solid lines for biotite/liquid and muscovite/liquid respectively) and serve for data representation in Figs. 7-12.

Figure 3. Geological map of the St Sylvestre leucogranite Complex (SSLC) and location of known pegmatites classified according to petrological and field observations.

Figure 4. Whole rock compositions of SSLC leucogranites. (a) Debon and Le Fort (1983) A-B major element diagram . (b)-(f) trace element data. Li, Ba, Rb, F and Nb/Ta (in ppm) are plotted as function of Cs (in ppm). Data are from this study (table 3) and Friedrich (1984). For data from this study, samples for which micas have been analysed are distinguished with larger diamonds.

Figure 5. Compositions of micas in leucogranites and pegmatites from the SSLC in the classification diagrams of A) Monier and Robert (1986) and B) Tischendorf et al. (1997). bi = biotite, mu = muscovite, znw = zinnwaldite, lep = lepidolite.

Figure 6. Trace elements contents (F, Li, Cs, Rb, Ba in ppm) and Nb/Ta ratio (in ppm) in micas from leucogranites and pegmatites. Values of Mg-Li are in a.p.f.u. bi = biotite, mu = muscovite, znw = zinnwaldite, lep = lepidolite.

Figure 7. Calculated trace elements contents (Li, F, Ba, Rb, Cs in ppm) of leucogranitic liquids at equilibrium with micas from granites (biotite: C_L^{bi}, muscovite: C_L^{mu}) plotted as a function of mica Nb/Ta values. In all plots, liquids have ranges of concentrations shown as bars since they are calculated by using the entire range of Kd values (see text). The marker on the bar corresponds to the arbitrary value calculated by using the preferred Kd value.

Figure 8. Calculated trace element contents (Li, F, Rb, Ba in ppm) of leucogranitic liquids at equilibrium with micas from granites plotted as a function of the calculated Cs concentration of the liquid ($[Cs]_{liq}$). C_L^{bi} = liquid at equilibrium with biotite, C_L^{mu}= liquid at equilibrium with muscovite. In all plots, liquids have ranges of concentrations shown as bars since they are calculated by using the entire range of Kd values (see text). The marker at the intersection of the bars corresponds to the arbitrary value calculated by using the two preferred Kd values.

Figure 9. Calculated trace elements contents (Li, F, Ba, Rb, Cs in ppm) of liquids at equilibrium with micas from pegmatites (biotite: C_L^{bi}, muscovite: C_L^{mu}) plotted as a function of mica Nb/Ta values.

Figure 10. Calculated trace element contents (Li, F, Rb, Ba in ppm) of pegmatitic melts at equilibrium with micas plotted as a function of the calculated Cs concentration of the liquid ($[Cs]_{liq}$). C_L^{bi} = liquid at equilibrium with biotite, C_L^{mu}= liquid at equilibrium with muscovite, C_L^{znw}= liquid at equilibrium with zinnwaldite; C_L^{lep} = liquid at equilibrium with lepidolite.

Figure 11. Calculated trace element contents $C_L^{(bi/mu)}$ of liquid at equilibrium with micas in granites compared to estimated evolution of liquid compositions in granites from C_0 to C_f.

Figure 12. Calculated trace element contents of liquid at equilibrium with micas C_L in pegmatites compared to estimated evolution from C_0 to C_f of liquid compositions in the pegmatites.

Figure 13. Incompatible element evolution of leucogranites and pegmatites from the SSLC and MAPF. For each rock, the $[Rb]_{liq}$ vs. $[Cs]_{liq}$ calculated from mica compositions values are compared with the calculated C_L values and the C_0 to Cf trend. Note that calculations are performed using only the preferred Kd values. Whole-rock data are also shown for comparison (for pegmatites only data for type VI). (a) leucogranites; (b) pegmatites; (c) leucogranites and pegmatites.